Thermoluminescence responses from europium doped gadolinium oxide

2006 J. Phys.: Condens. Matter 18 9257

(http://iopscience.iop.org/0953-8984/18/40/011)

INSTITUTE OF PHYSICS PUBLISHING JOURNAL OF PHYSICS: CONDENSED MATTER

J. Phys.: Condens. Matter **18** (2006) 9257–9272 doi:10.1088/0953-8984/18/40/011

Thermoluminescence responses from europium doped gadolinium oxide

Y Wang[1,2], O Milosevic[3,4], L Gomez[4], M E Rabanal[4], J M Torralba[4], B Yang[1,2] and P D Townsend[2,5]

[1] Department of Physics, Beijing Normal University, Beijing 100875, People's Republic of China
[2] Science and Technology, University of Sussex, Brighton BN1 9QH, UK
[3] Institute of Technical Sciences of Serbian Academy of Sciences and Arts, 11000, Belgrade, Serbia
[4] University Carlos III, Madrid, Spain

E-mail: p.d.townsend@sussex.ac.uk

Received 31 July 2006, in final form 4 September 2006
Published 22 September 2006
Online at stacks.iop.org/JPhysCM/18/9257

Abstract

Thermoluminescence signals and morphological studies are reported for a new phosphor of Gd_2O_3. The phosphor particle material was synthesized by an aerosol technique and it is heavily doped with Eu. Annealing at 1200 °C increases the luminescence efficiency by ∼1000-fold relative to the as-prepared material. The emission spectra are primarily from the red transitions of the Eu, but weaker short wavelength emissions can also be detected during low temperature thermoluminescence. There are numerous wavelength dependent differences between the low temperature thermoluminescence curves. These variations are interpreted to show that there are a range of defect and luminescence sites in the Gd_2O_3:Eu phosphors. These are associated with the symmetry of the crystal field around the europium ion, which is a function of the phase content, i.e. resulting from sample preparation and annealing. The sites are almost independent in terms of their emission spectra, but the stability of some sites is enhanced by the presence of Eu so that the TL peaks appear at higher temperatures than the intrinsic defect TL of the host material. The synthesis of uniform and submicron sized spherical particles with nano-clustered inner structure is demonstrated with various analysis techniques (XRPD, FE-SEM and HR-TEM). The effect of processing parameters and post-annealing treatment is discussed from the viewpoint of different phase formation.

(Some figures in this article are in colour only in the electronic version)

[5] Author to whom any correspondence should be addressed.

1. Introduction

As part of a programme to develop high grade phosphors in the form of particles with a narrow size distribution, a spherical morphology and absence of agglomerates, efforts have been made to prepare material using an aerosol approach [1–3]. Success in this fabrication has recently been demonstrated with europium doped gadolinium oxide [4]. The gadolinium oxide host can be grown with high levels of europium and the particles produce intense red emission from the europium sites in the lattice. However, as initially fabricated the material lacks intensity and requires thermal treatments. The sensitization of the as-grown material is a critical stage in the preparation of the phosphor and sensitivity improves with annealing at temperatures above 800 °C. The signals increase even further with higher temperature treatments, of 12 h duration up to temperatures of at least 1200 °C. One may consider several reasons for the changes which provide the sensitization. Speculations include removal of unwanted trace materials incorporated during the fabrication process, improvements in the crystallinity of the mixture, alterations in surface sites of the particles and dispersion and homogenization of the Eu dopants within the particles.

Further information on the thermally induced changes is included here, as we will report that the phase of Gd_2O_3:Eu changes with annealing temperature. This can be a contributory factor to the luminescence efficiency. There is a very limited literature for the aerosol prepared material, and earlier results [4] were obtained with a sample composition with a Gd to Eu ratio of 9:1. Such substantial dopant levels are desirable in that they offer a high concentration of sites for Eu luminescence, but, equally, high dopant conditions have the potential to result in clustering of the Eu ions into non-radiative sites. In general, the lattice strains of dopant inclusions can of course generate intrinsic defects or induce phase separation and/or precipitation of the dopant ions into interacting clusters. All such scenarios can result in greatly reduced luminescence efficiency.

Since the earlier results clearly showed that the emission intensity was greatly increased by annealing, it suggested that one had not reached a Eu dopant saturation limit for the phosphor. Therefore, the present material preparation used a higher dopant concentration of Gd:Eu of 8:2.

In addition to the luminescence data it is essential to quantify aspects of the structure and morphology as these are crucial factors for a reproducible phosphor. Particle structure and the morphology results of the sample will be shown here. Several microscope techniques were used to show variations of the structure with heat treatment; for example, a monoclinic phase was observed after the sample powder was annealed above 1100 °C.

2. Experimental details

The samples were prepared as described previously [4] from solutions of $Gd(NO_3)_3{\cdot}x6H_2O$ and $Eu(NO_3)_3{\cdot}x6H_2O$ to obtain 0.080:0.020 Gd/Eu molar ratio. The solutions were atomized ultrasonically (piezo-transducer resonant frequency of 2.1 MHz), introduced into a high temperature tubular flow reactor with air as a carrier gas, and decomposed at 700 °C. The gas flow rate was 1.5 l min^{-1}, and the corresponding droplet/particle residence time was 75 s. This resulted in a fine powder called 'as prepared', which was subsequently thermally annealed. Annealing was performed in air at temperatures of 800–1200 °C for periods of 12 h.

The TL emission spectra were registered by a high sensitivity system employing wavelength multiplexed spectrometers [5]. The data of the recorded spectra were corrected for the wavelength sensitivity of the spectrometer and detector system. Note that as the spectrometer system is wavelength multiplexed the entire spectral range is recorded simultaneously at each temperature, thus any variations in peak temperature with wavelength

are meaningful. Above room temperature spectra were taken at a heating rate of 0.5 °C s^{-1}, whereas for the low temperature data a lower heating rate of 0.1 K s^{-1} was used in order to avoid thermal gradients across the samples. The samples were in the form of powder which was fixed on Al discs with vacuum grease. The TL was excited by x-ray irradiation with 40 kV x-rays. The radiation dose for high temperature TL was typically 200 Gy, and similarly for the low temperature TL. Since the emission spectra could be recorded during irradiation some measurements of radioluminescence (RL) were also acquired.

The crystal phases and particle morphology of as-prepared and annealed samples were determined by x-ray powder diffraction (XRD), field emission scanning electron microscopy (FE-SEM) and transmission electron microscopy (TEM). XRD patterns were recorded with Cu Kα radiation in an X'Pert Philips automatic diffractometer. The 2θ range analysed was 10°–100° with a step scan of 0.02 and a counting time of 11 s for each step. The working conditions were 40 kV and 40 mA. All peak positions were used for the determination of microstructural parameters. Structural refinements were carried out using the Rietveld based program Fullprof. A FESEM was used in order to identify particle morphology. The samples were prepared by dispersion of a small powder portion into acetone and spreading it on a glass surface, and then coating it with carbon. Several acceleration voltages were tested. The best images were obtained with 5 kV and a 3.3–3.9 mm working distance. Analytical and TEM investigations were performed with a Philips TECNAI 20 FEG operating with 200 kV equipped with EDX TEM Quant and a point resolution of 2.0 Å. TEM samples were prepared by ultrasonic dispersion of a small powder portion in acetone and dispersion of this suspension on a carbon coated 3 mm of diameter copper grid.

3. Thermoluminescence results

Thermoluminescence (TL) glow curves contain information regarding the release of charge from trapping sites at different temperatures, which is related to the trap depth. Additionally, measurement of the emission spectra can reveal differences between the types of recombination site and/or distinguish between electron and hole release. Consequently, TL data are sensitive to effects of thermal treatments, defect concentrations and association of defect complexes. The previous work presented the emission spectra taken during TL [4]. The current samples include a higher Eu dopant concentration and this modifies the types of defect which exist, and the changes are evidenced by alterations of the TL curves. TL signals were collected both at temperatures above room temperature and in the low temperature range between 25 and 280 K. Note that the TL literature emphasizes that lower temperature data are well suited to detect changes in both intrinsic and dopant emission sites. Indeed, effects were seen here both for the changes in Eu concentration, the responses of intrinsic defects and the effects of high temperature annealing.

Overviews of the spectral data of intensity as a function of emission spectra and temperature are conveniently displayed as a combination of isometric plots and contour maps, since these images define the general pattern of the emission. More quantitative data are presented as slices from the isometric information and slices can be prepared to show emission spectra at a specific temperature, or the TL glow curves as a function of wavelength. There are major differences in intensity between the short wavelength signals and those from the europium sites. For the weak signals, rather than use a single wavelength or temperature channel for the slices, the signals were integrated over a range of temperature or spectral channels.

Figure 1 contrasts the high temperature isometric plots of the TL for material as originally prepared with samples which had been annealed for 12 h at 1200 °C. As is immediately

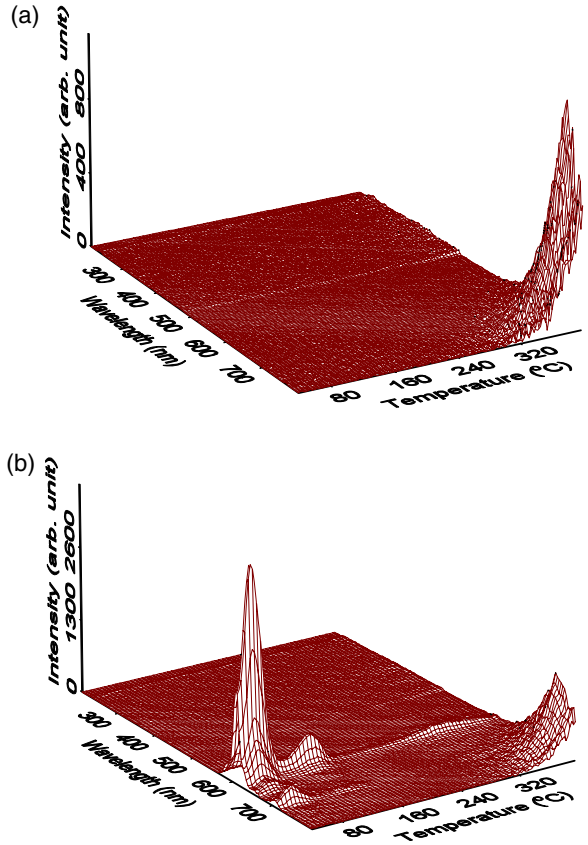

Figure 1. Isometric views of the TL spectra of Gd_2O_3:Eu after x-ray irradiation at room temperature. The left hand image corresponds to the 'as-prepared' powder and the right one to powder that had been annealed at 1200 °C.

obvious, the initial signals from the 'as-prepared' samples are virtually non-existent and the major feature on the figure is from the black body thermal emission. However, after annealing, the samples provide intense TL features with sharply defined red emission bands. The bands are at wavelengths characteristic of Eu transitions but the Eu lines are broadened in the Gd_2O_3 host relative to those from atomic spectra. This emphasizes that the radiative decay pathway is primarily via the dopant ions. Figure 1 shows that annealing has increased the efficiency by around one thousand-fold. A contour map of the intensity pattern for the Eu signals is shown in figure 2(a). There is a very large intensity range between the various Eu inner shell transition lines and figure 2(b) displays a simple spectrum. One notes that there are some minor wavelength shifts and also obvious changes in the relative transition intensities after annealing. These were apparent at anneal temperatures above 800 °C, and the example shown here contrasts the original as-prepared spectrum with that after a 1200 °C anneal. Both signals were recorded above room temperature. One notes that such changes in the inner shell rare earth transition spectra are typical as being the result of changes in the local crystalline field, hence the data suggest that some structural relaxation and/or phase transition has occurred as the result of the high temperature anneals. Figure 3 shows a conventional TL curve for signals recorded at two of the europium emission wavelengths. Once normalized, the 610 and 705 nm

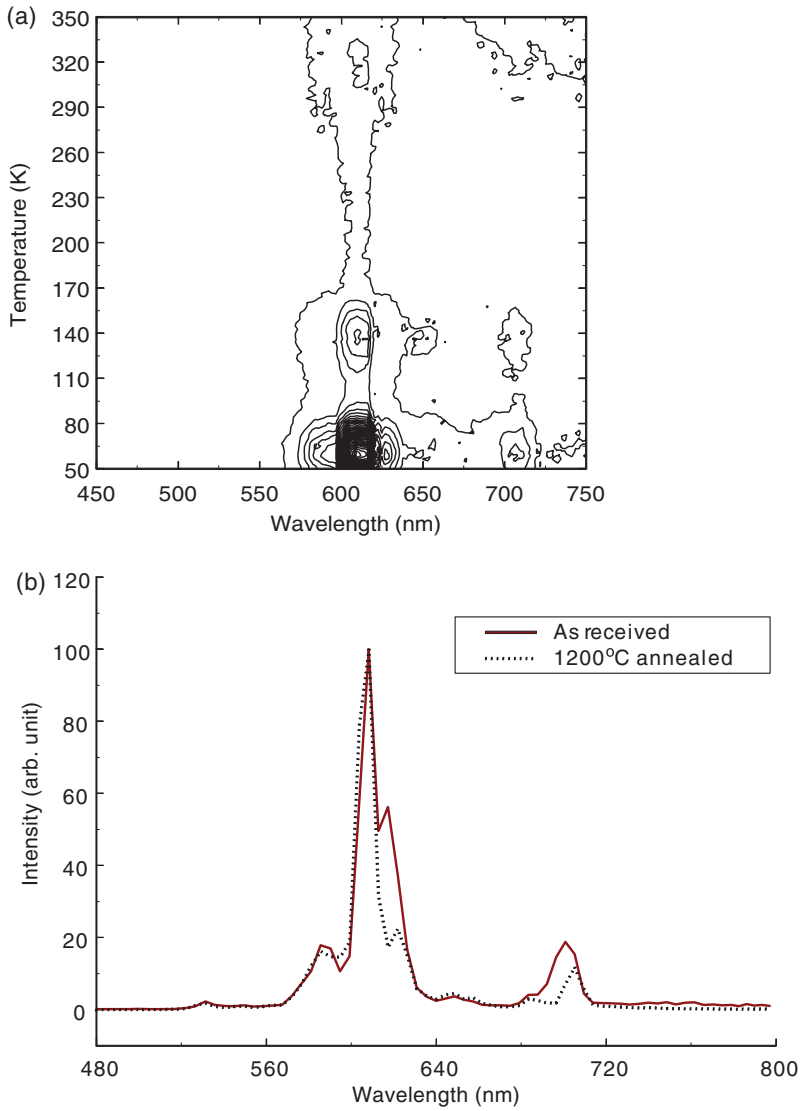

Figure 2. (a) A contour map of the TL intensity above room temperature from a sample which had been annealed at 1200 °C. (b) Radioluminescence spectra from Eu in the 'as-prepared' sample and from material annealed at 1200 °C.

TL graphs have the same form, but the longer wavelength signal is distorted above ∼300 °C by the rising black body emission.

The low temperature TL was recorded from 25 K and here there are a number of features in the UV/blue region of the spectrum, as well as from the europium dopant sites. Examples of the isometric plots are given in figure 4 together with examples of contour plots in figure 5. Note that the apparent intensity step near 450 nm for the unheated sample data is merely an artefact of the use of two detector regions. Intensity matching between detectors for such weak signals has not been attempted as there is a very large intensity range between the signals at the short wavelengths and in the red region. This intensity difference is dealt with in

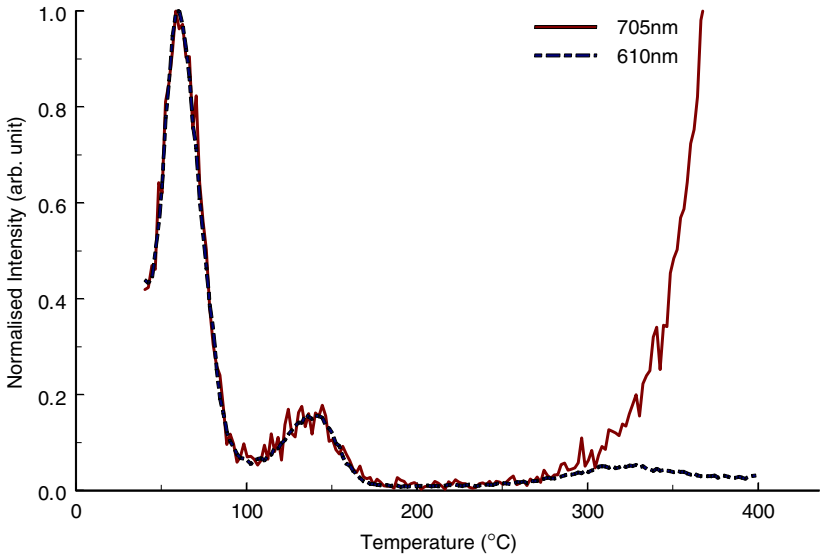

Figure 3. TL curves above room temperature for a 1200 °C annealed sample (note that for the 705 nm signal the high temperature values are dominated by the black body radiation).

figure 5 by displaying the short and long wavelength data as separate contour plots. As for the room temperature examples there are major intensity differences between signals from the 'as-prepared' material and samples which had been annealed. The examples shown here are for the material after the 1200 °C anneal but the data from the material annealed at either 900 or 1000 °C are quite similar, albeit slightly less intense. The most obvious change as the result of annealing the samples is that the Eu signals dominate the spectra.

Figure 4 also shows the effects of 1000 °C annealing both for the material with the Gd:Eu ratio of 8:2 and the earlier material with a ratio of 9:1. After annealing the spectra are again dominated by the red line spectra from Eu transitions. The TL glow peaks appear at comparable temperatures but the relative intensities of the peaks are a function of Eu concentration and anneal temperature. In particular, the 1000 °C anneal does not clearly resolve the TL peaks. For the more lightly doped sample (9:1) the first of the main peaks is considerably weaker and the pair of higher temperature peaks is replaced by a weak and continuous emission during the heating.

Information regarding defect and luminescence sites is provided by TL data in different spectral regions and figure 6 emphasizes these variations with normalized intensity plots. Since the temperatures of the glow peaks differ with wavelength one can conclude that there are several independent recombination sites which are linked to specific types of charge trap. This conclusion is quite different from the simplistic models of TL where charge trapping and recombination centres are totally independent. There are various overlapping peaks and table 1 summarizes the nominal peak values as a function of wavelength for the annealed sample. No attempt has been made to deconvolute the features into detailed component TL peaks. Some of the features are broad and asymmetric, which may indicate that there are several components. Approximate intensity values are included in the table, with the weakest peak defined as unit intensity.

Figure 6(a) sketches the normalized TL glow curves as recorded in five different wavelength regions. The figure, and table 1, show identical TL glow curves (within

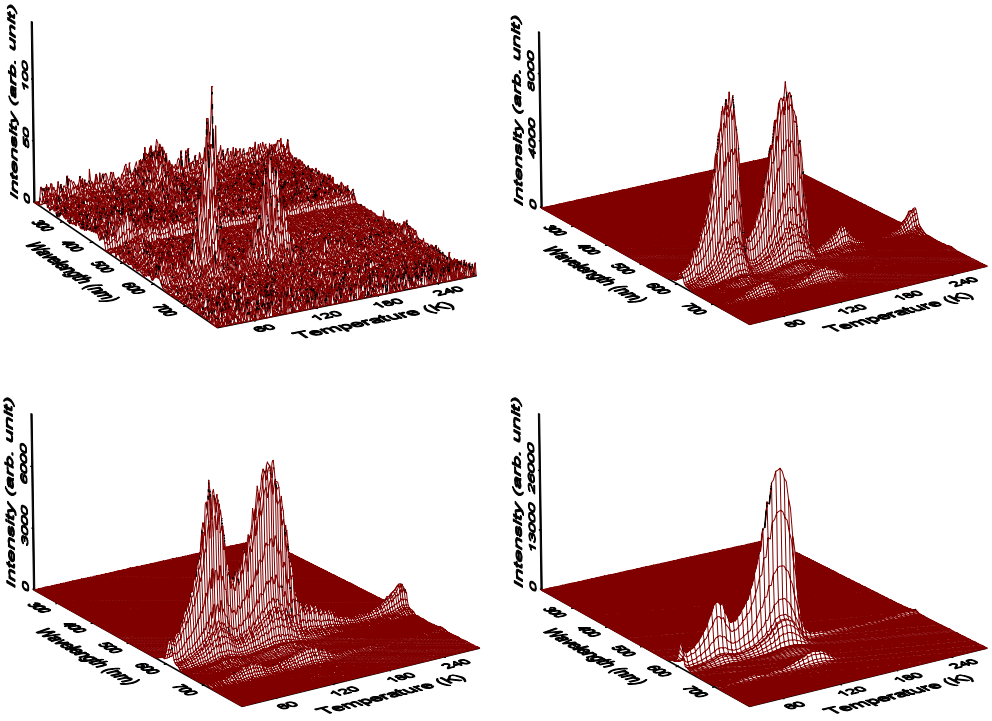

Figure 4. Low temperature TL emission spectra of Gd_2O_3:Eu. Upper left shows the TL for an 'as-prepared' sample with Gd:Eu ratio of 8:2 and the upper right values are after the 1200 °C anneal. The lower figures are after 1000 °C anneals, where the lower left example for a sample with the Gd:Eu ratio of 9:1 and the lower right for the ratio of 8:2.

Table 1. TL peaks which appear at low temperature for a 1200 °C annealed sample.

Wavelength (nm)	TL peak (K)							Relative intensity						
250–350		77		125					1		3.5			
350–400	48	77	98	125				1.2	1.9	1	2.7			
400–480	48	77	98	125				1.8	1.1	1.6	1			
570–670		77			137	198	280		8			8.3	1	1
670–750		77			137	198	280		8.2			8.3	1	1

experimental error) that appear for all the Eu transitions in the red spectral region. The Eu curves differ distinctly from those obtained from shorter wavelength analyses. Indeed, there are differences between all the shorter wavelength TL curves and a substantial difference in peak temperature from 125 to 137 K for the UV/blue emissions and the red Eu signals.

In intensity terms, annealing has only enhanced the europium emission and the UV/blue signals do not increase, although there are some changes in the relative intensities of the short wavelength TL peaks after the heat treatment. The Eu spectrum from these annealed samples is constant, within experimental error, from the low temperature data through to the high temperature TL, and matches that seen in the radioluminescence data of figure 2(b).

The contour plots of figure 5 do not readily reveal the details of the spectra at the shorter wavelengths so figure 7 contrasts the short and long emission spectra. Figure 7 presents the

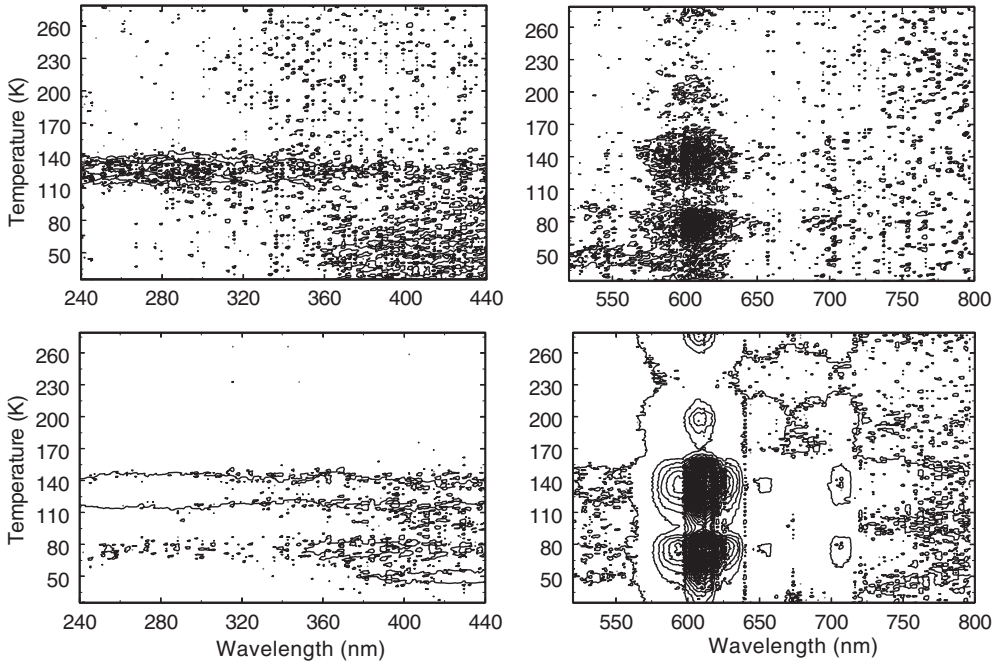

Figure 5. Low temperature contour data of the TL from samples 'as prepared' (upper figures) and after the 1200 °C anneal (lower figures). Note that the UV/blue and red regions are separated to accommodate their very large intensity differences.

Table 2. TL peaks which appear at low temperature for an un-annealed sample.

Wavelength (nm)	TL peak (K)							Relative intensity						
250–350				127							1			
350–400	48			127				1			1			
400–480	48		96	127				4		1	1.3			
500–570	48	85						3	1					
570–670		77			137			1.5				1		

short wavelength data from both TL at 60 and 130 K. The short wavelength radioluminescence spectrum at 130 K for the 1200 °C annealed Gd_2O_3:Eu particles is shown, but this is relatively featureless.

For the 'as-prepared' material one suspects that the same glow peaks are present at the same temperatures, as indicated by three TL patterns for three wavelengths in figure 6(b), but there are obvious differences in relative intensity compared with the annealed samples, not only between the short and long wavelengths, but also between the signals in the short wavelength region. Table 2 summarizes the pattern and indicates the approximate intensity pattern and figure 6(b) shows three wavelength examples of the TL glow curves.

4. Particle structure and morphology

XRD patterns implied the presence of two cubic phases in as-prepared powder sample formed during the aerosol process, a main $Ia\bar{3}$ phase and a secondary $Fm\bar{3}m$ phase with

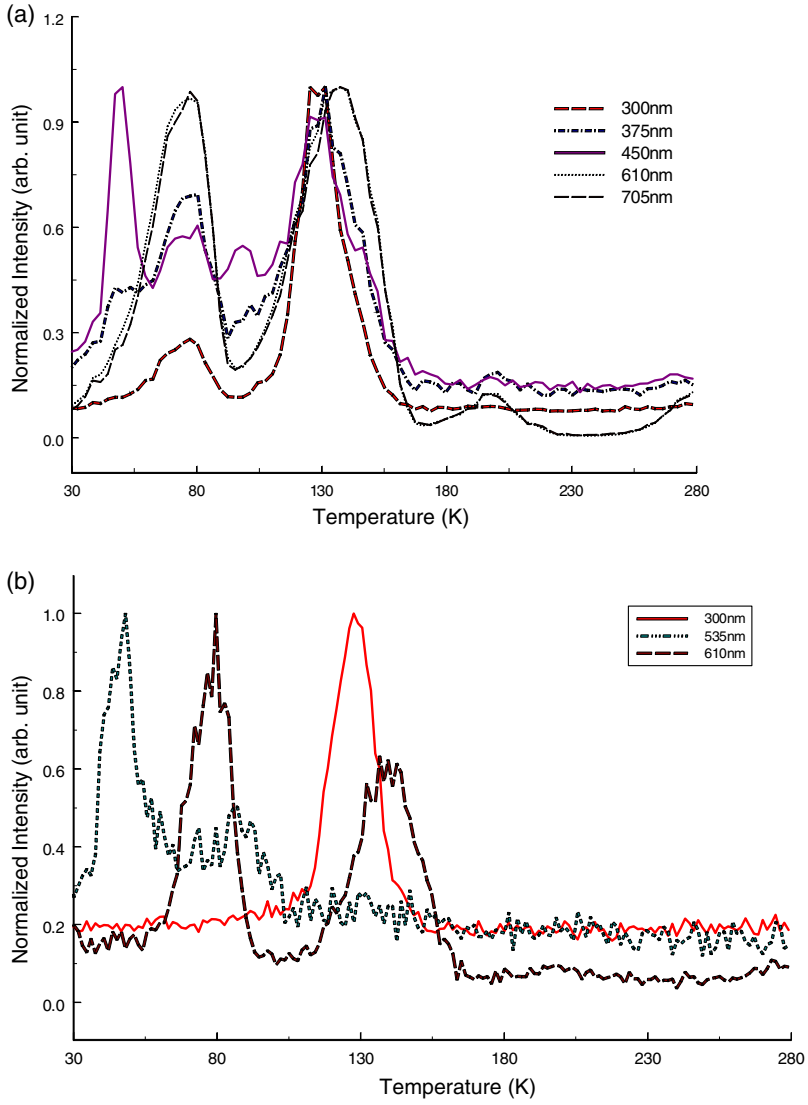

Figure 6. (a) Examples of the wavelength dependence of TL curves from Gd_2O_3:Eu after 1200 °C annealing. (b) Examples of the wavelength dependence of TL curves from 'as-prepared' Gd_2O_3:Eu.

the concentration of 12 wt%. The latter phase is structurally similar to the $Gd_2Te_6O_{15}$ (file card 37-1400, $a = 5.611$ Å) [4]. Table 3 summarized the derived lattice parameters, together with Rietveld based *Fullprof* refinement parameters. Only the $Ia3$ phase after the annealing was found. Based on XRD data evaluation, it is evident that the higher value of the cell parameter by comparison with the c-Gd_2O_3 ($a = 10.81$ Å, JCPDS file card 43-1014) indicates the incorporation of Eu^{3+} into the gadolinia matrix, since the Eu^{3+} ionic radius is slightly larger than Gd^{3+} (Eu^{3+}—0.095 nm; Gd^{3+}—0.094 nm). The differences in the luminescence changes for as-prepared and thermally treated samples could therefore be related to changes in the gadolinia crystal structure, i.e. the existence of two cubic phases in as-prepared samples and only cubic $Ia3$ after annealing (as evidenced by XRD).

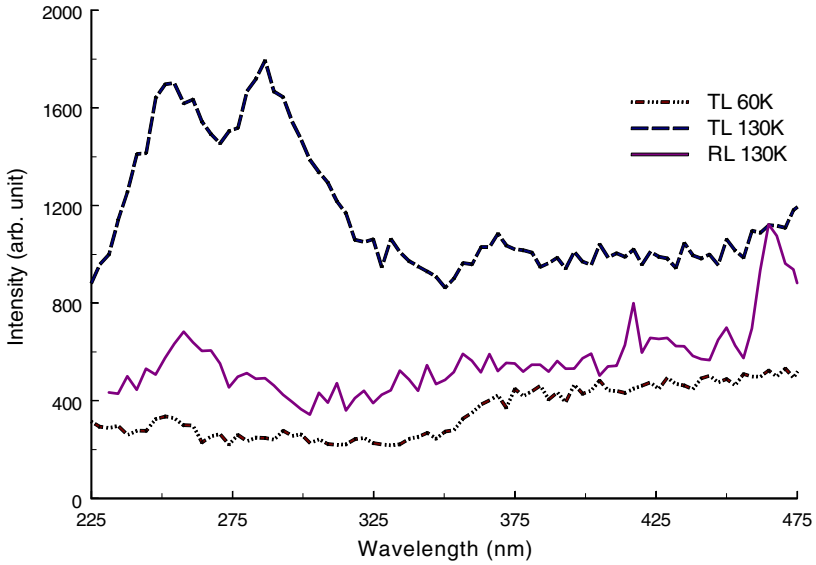

Figure 7. TL spectrum at 60 and 130 K, and RL spectra at 130 K of 1200 °C annealed Gd_2O_3:Eu in the short wavelength region.

Table 3. Rietveld based *Fullprof* refinement parameters.

Temperature °C /time (h)	Phase	Lattice parameter (Å)	Rp (%)	Rwp (%)	Rf (%)	Rb	χ^2
As prepared, 700	$Ia3$	10.835(1)	11.1	14.2	8.93	9.88	2.82
As prepared, 700	$Fm\bar{3}m$	5.620(1)	11.1	14.2	10.1	13.9	2.82
800/12	$Ia3$	10.822(1)	11.60	15.6	25.4	14.4	1.5
900/12	$Ia3$	10.821(1)	11.60	15.6	25.4	13.9	1.5
1000/12	$Ia3$	10.818(1)	12.9	16.9	26.7	20.4	1.58
1100/12	$Ia3$	10.821(2)	13.6	17.6	34.8	22.0	1.71
1200/12	$Ia3$	10.8360(4)	10.3	14.0	14.7	8.78	1.70

Since an important factor for the phosphor preparation is the form of the particles, figure 8 shows a high resolution FE-SEM image of the as-prepared and thermally treated powder samples. The secondary particles have spheroidal geometry, in the submicrometre range. These tend to agglomerate either as chains or clusters of particles of primary nano-particles, particularly as the result of the annealing treatments. FE-SEM images clearly show the differences in the particle morphology depending on their preparation history. On increasing the annealing temperature, the particle surfaces become smoother, which may indicate either a phase transition or other primary particle rearrangement. Loosely sintered primary particles are evident inside agglomerates at 1000 °C. However, at higher temperature (figure 8(c)), interparticle collision and sintering are evident among the secondary particles, followed by decreases of the primary particle size dispersion, to smaller particles.

TEM additionally revealed the morphological changes and changes in particle association for the 'as-prepared' and thermally treated particles. Based on the low magnification bright field image (figures 9(a)–(d)), it is again evident that annealing tends to allow association of the particles.

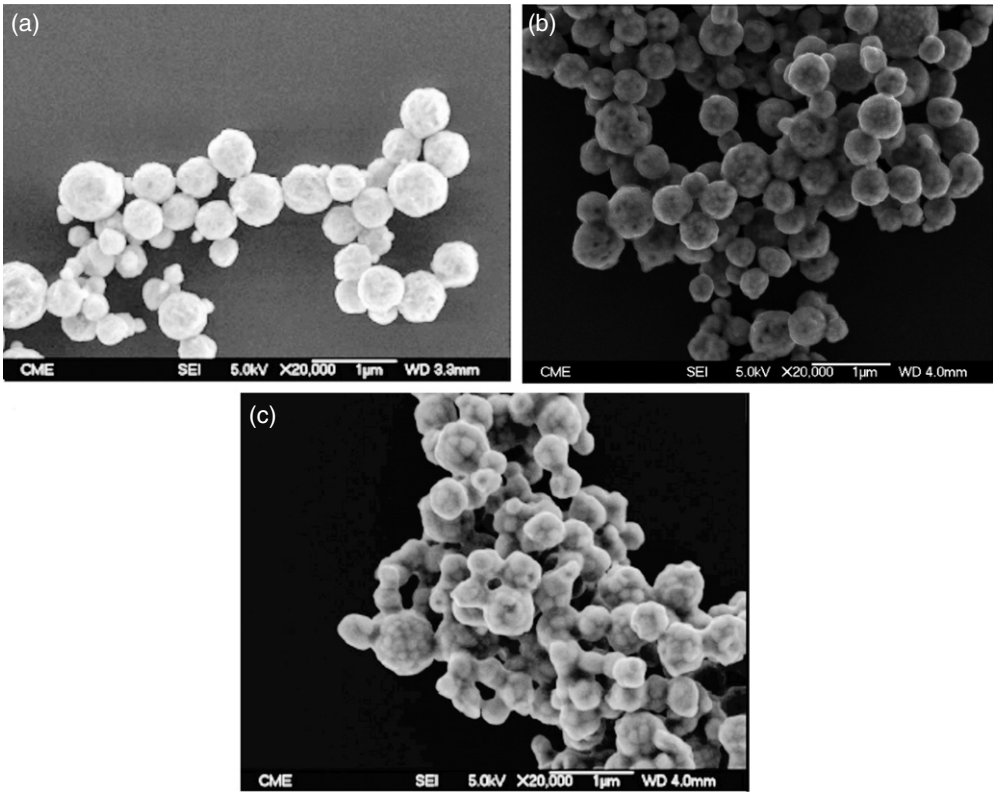

Figure 8. FESEM of the as-prepared Gd_2O_3:Eu particles with (a) initial powder samples, (b) after annealing at 1000 °C for 12 h and (c) after 1100 °C for 12 h.

SAED patterns confirmed the results of XRD analysis, showing two polycrystalline cubic phases in 'as-prepared' samples: the main phase is bcc with $Ia3$ space group, and the unit cell parameter $a \approx 10.8$ Å; the secondary phase has $Fm\bar{3}m$ symmetry and the cell parameter of 5.6 Å. In samples treated at temperatures of 800–1000 °C for 12 h, only the cubic $Ia3$ phase has been observed (figures 9(b)–(d)). However, the detailed TEM observations revealed the existence of a well ordered phase for the samples treated at 1100 °C for 12 h (which was not observed in the XRD patterns). The new phase is different from the cubic one, and the interplanar spacings indicate a similarity with a monoclinic phase.

The details of this minority phase can be appreciated in figure 10, where an HR-TEM image in bright field of the sample treated at 1100 °C for 12 h shows the periodicity and an ordered structure. The inset in the same picture represents the fast Fourier transform (FFT), indexed according to a $C2/m$ symmetry, that was also confirmed with SAED patterns (figure 9(d)), indicating a monoclinic phase with the approximate unit cell parameters $a = 13.6$, $b = 3.56$, $c = 8.6$ (a:b:c = 3.82:1:2.41), $\beta = 100.6°$. This phase is equivalent to the file card JCPDS = 43-1015 and the results obtained are summarized in table 4, together with the interplanar spacings, and the hkl Miller indices, taken from several SAED patterns or directly obtained from the FFT of the images. It is evident that there is a good agreement between measurements and the theoretical values (JCPDS 43-1015). The defects formed along the grain boundaries, easily resolved in the same image, could be responsible for extra spots that are present in FFT of some areas of the image.

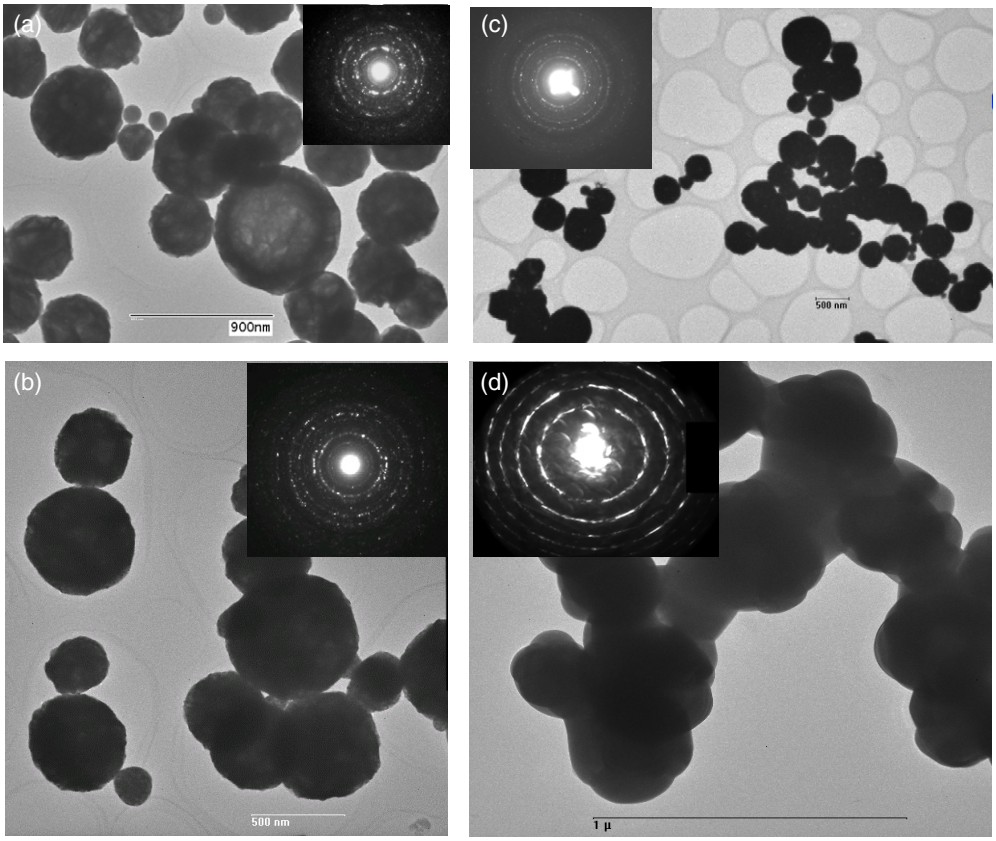

Figure 9. TEM of the Gd_2O_3:Eu particles, (a) as prepared, (b) powder samples annealed at 800 °C for 12 h, (c) 900 °C for 12 h and (d) 1100 °C for 12 h.

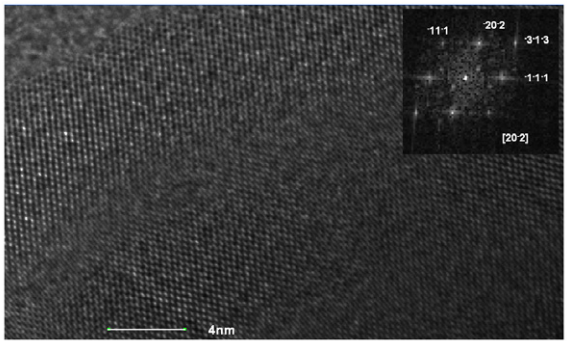

Figure 10. HR-TEM image in bright field of the powder sample treated at 1100 °C for 12 h together with the FFT, indexed according to a $C2/m$ symmetry along the $[20\bar{2}]$ axis zone (in inset).

Figure 11 represents an HR-TEM Fourier filtered view of the above image, and the corresponding fast Fourier transform (FFT) (included as an inset), indexed according to a monoclinic $C2/m$ phase along the $[20\bar{2}]$ axis zone. In the image the (111) and the (202) planes are resolved. Figure 12 represents a comparison between the calculated electron diffraction

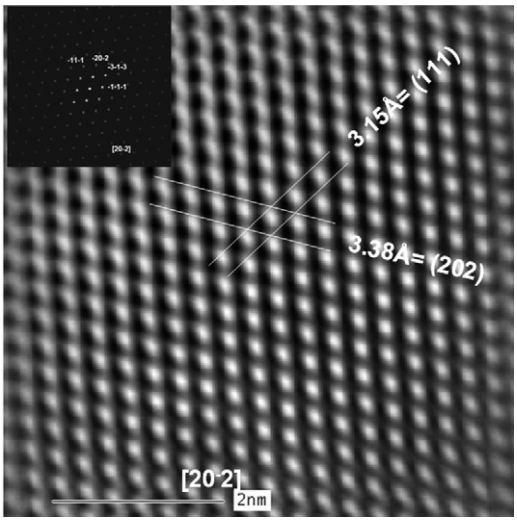

Figure 11. Fourier filtered HR-TEM of the above image and the corresponding FFT (in inset), indexed according to a monoclinic $C2/m$ phase along the $[20\bar{2}]$ axis zone.

Table 4. The theoretical and empirical parameters of the monoclinic phase identified after annealing at 1100 °C for 12 h.

	JCPDS 43-1015	Experimental	*hkl* Miller indices
Space group	12 $C2/m$	12 $C2/m$	
Lattice parameters	$a = 14.06$, $b = 3.55$, $c = 8.56$	$a = 13.6$, $b = 3{,}56$ $c = 8.6$	
Angles	$\alpha = \gamma = 90°$ $\beta = 100.1°$	$\alpha = \gamma = 90°$ $\beta = 100.6°$	
Interplanar distances	d (Å)	d (Å)	h k l
	8.62	8.6	0 0 1
	4.312	4.31	0 0 2
	3.158	3.15	1 1 1
	2.875	2.86	0 0 3
	2.755	2.739	−1 1 2
	2.431	2.43	4 0 3
	2.131	2.1	−3 1 3
	1.913	1.91	3 1 3

pattern, in accordance with the procedure of Morniroli *et al* [6], and the FFT is shown as well, indicating a good agreement between both images according to the $C2/m$ model.

For the case of the rare earth sesquioxides, a monoclinic phase is metastable at ambient conditions and could be obtained by quenching from high temperatures and under high pressure [7]. However, a short residence time and high heating rates associated with the aerosol route may favoured to the formation of the metastable monoclinic structure at temperatures $\geqslant$1100 °C. Similar observations are reported in the case of the Y_2O_3:Eu^{3+} phosphor system obtained through the gas phase, where the monoclinic phase was resolved in the particles less than 20 nm [1, 8]. The stabilization of the higher density metastable monoclinic structure is probably attributable to the Gibbs–Thomson effect, in which the increased surface tension, as a characteristic of nano-particles, converts the particle to the denser metastable phase [7]. This phase obviously appears locally in the examined Gd_2O_3:Eu^{3+} system, having short distance order and being invisible for XRD, however visible on TEM observations.

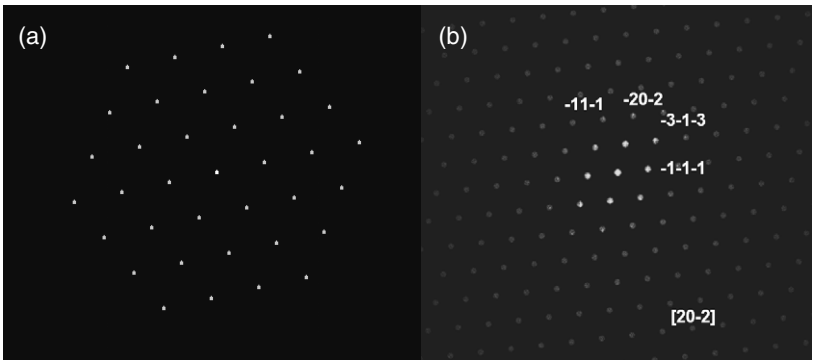

Figure 12. A comparison between (a) the calculated electron diffraction patterns and (b) FFT for the $[20\bar{2}]$ axis zone.

The monoclinic phase has space group $C2/m$ and the lattice possesses three crystallographically distinct cation sites, each having point group symmetry Cs. All three cation sites are sevenfold coordinated [9, 10]. Thus, the Eu^{3+} occupies the three non-equivalent crystallographic sites in the monoclinic structure. For the case of the Gd_2O_3:Eu^{3+} cubic crystalline system, with space group $Ia3$, the Eu^{3+} ion can occupy two Gd^{3+} sites with a coordination number of 6 with C_2 and S_6 symmetries [11, 12].

When introduced into the solid gadolinia, the Eu^{3+} luminescence is associated with both 4f–4f intrashell and $^5D_0 \rightarrow {}^7F_j$ ($j = 0$–4) intershell transitions. Since the 4f levels are unaffected by the host lattice, the shape and symmetry of the d orbitals have essentially five orientations, so the energy level positions associated with each orientation depend on the local crystalline field surrounding the Eu^{3+} ion [13]. These changes affect the luminescence spectra and relative line intensities, as already noted. The luminescence spectra of the Eu^{3+}-doped gadolinia for the sample annealed at 1200 °C, as shown in figure 2(b), correspond to $^5D_0 \rightarrow {}^7F_j$ ($j = 0$–4) transitions. The most intense component for the set of $^5D_0 \rightarrow {}^7F_2$ transitions is observed near 610 nm and this emission is characteristic of the C_2 symmetry site in the cubic $Ia3$ phase, as seen for the 1200 °C annealed samples (figure 1). The local appearance of the metastable monoclinic phase at temperatures above about 1100 °C is associated with a high content of interfaces and high defect content. These changes may cause broader luminescence lines, as the result of Eu^{3+} in a locally disordered gadolinium oxide matrix.

5. Discussion

The results shown above are interesting in that they show that increasing the europium content of the phosphor can modify the types of defect site which exist within the phosphor and that the overall emission intensity can be increased by ∼1000-fold by high temperature annealing. Very high dopant concentrations are considered here, of up to 20% of the Gd sites, but the fact that this is feasible is not surprising. Gd and Eu rare earth ions are adjacent members of the periodic table and differ in ionic radius by no more than 1%. The more important factor on the lattice distortion is defined by the ionic volume difference and even this is only ∼3%. At such high dopant concentrations there will be strong coupling between dopant sites. Long range interactions between defects (including dopants) must be considered [14, 15], and examples have been established over as many as 25 neighbouring ionic shells. Thus strong coupling between Eu sites is expected for the present heavily doped material. For many types of dopant,

coupling offers routes for energy transfer between sites which would quench the luminescence. Surface quenching is also a factor to consider, so efficiency is a function of particle size (e.g. as discussed in a recent review [16]).

For the annealed samples there is no obvious evidence for Eu concentration quenching, perhaps because the Eu inner shell transitions are sufficiently screened that the luminescence is still a favoured energy decay path. Hence the Eu transitions of the thermoluminescence signals are intense. Conversely, the 'as-prepared' samples show only weak TL signals because of a much higher concentration of intrinsic defect sites which can quench the luminescence or inhibit charge retention during the irradiation stage. High intensity TL, which occurs preferentially at Eu sites, may indicate that the stored charges resulting from the x-ray ionization within the lattice are trapped at sites which directly involve Eu ions. The concept of defect complexes which provide both the trapping and luminescence sites has been proposed for many TL materials, including standard radiation dosimeters such as LiF:Mg:Ti:O (TLD100) or CaF_2 etc [17] and minerals such as $CaCO_3$:Mn [18].

The gadolinium oxide TL results further confirm this pattern of behaviour since the UV/blue emission TL signals generate low temperature glow curves which differ in temperature and the number of component TL peaks from signals arising from the rare earth dopant ions. Indeed, the responses very closely match the TL behaviour of LaF_3 [19, 20] and bismuth germinate (BGO) [21] doped with rare earth ions. In each of these cases the intrinsic TL of the host lattice is seen at low temperature at short wavelengths and includes several TL peaks below about 130 K, corresponding to annealing of intrinsic defects. The 130 K value is characteristic of the upper temperature limit for annealing of hole type defect traps [19]. Variants of these same defect structures which involve the rare earth dopants have altered charge stability and the TL peak temperatures rise with the size mismatch of the dopant from the host lattice site. The peak temperature shift (tables 1 and 2) from ∼125 to 137 K from intrinsic signals to the Eu emission TL is in line with the LaF_3 and BGO examples. Similarly to the LaF_3, the gadolinium oxide shows a more complex number of TL peaks with increasing rare earth content [20], as exemplified in figures 1 and 4. Figures 6(a) and (b), and the two tables, also indicate that the TL glow curves are very different for the Eu signals, the 'as-prepared' and annealed samples. These differences may be interpreted as yet further evidence that, whilst the charge trapping sites have generically the same type of defect structure in each case, the detailed differences between the sites result in not only different emission spectra but also different TL temperatures.

6. Summary

An aerosol route was applied for the synthesis of nanostructure submicron sized spherical Gd_2O_3:Eu^{3+} particles. The particle morphology and phase content were evaluated by different analysis techniques (XRPD, FE-SEM and HR-TEM) and discussed in terms of the processing parameters and post-annealing temperature. XRD patterns implied the presence of two cubic phases in as-prepared powder: a main $Ia3$ phase and a secondary $Fm\bar{3}m$ phase with the concentration of 12 wt%. Only the $Ia3$ phase after the annealing was found. HR-TEM investigations proved the local appearance of the metastable monoclinic $C2/m$ structure at temperatures around 1100 °C, whose formation is probably associated with the high heating and cooling rates during synthesis. In conclusion, the TL signals demonstrate that there are numerous defect and luminescence sites in the Gd_2O_3:Eu phosphors which are a function of sample preparation, dopant concentration and annealing. The sites are somewhat independent in terms of their emission spectra, and the stability of some sites is enhanced by the presence of Eu so that the TL peaks appear at higher temperatures than those of the host material.

Acknowledgments

This research is financially supported though The Ministry of Science and Environment Protection, Republic of Serbia (project No 142010) as well as through COST 539 Action. The authors gratefully acknowledge Dr Luis Pebla, the Director of the Microscopy Centre of the Universidad Complutense de Madrid, and Ivan Luis Baldonedo for the technical support of the SEM observations. One of the authors, OM, gratefully acknowledges the support of the Ministry for Education and Science, Spain, for the sabbatical grant SAB 2004-0035.

References

[1] Dosev D, Guo B and Kennedy I M 2006 Photoluminescence of Eu^{3+}:Y_2O_3 as an indication of crystal structure and particle size in nanoparticles synthesized by flame spray pyrolysis *Aerosol Sci.* **37** 402–12

[2] Jung D S, Hong S K, Lee H J and Kang Y C 2006 Gd_2O_3:Eu^{3+} phosphor particles prepared from spray solution containing boric acid flux and polymeric precursor by spray pyrolysis *Opt. Mater.* **28** 530–5

[3] Joffin N, Caillier B, Garcia A, Guillot P, Galy J, Fernandes A, Mauricot R and Dexpert-Ghys J 2006 Phosphor powders elaborated by spray pyrolysis: characterizations and possible applications *Opt. Mater.* **28** 597–601

[4] Milosevic O, Mancic L, Rabanal M E, Yang B and Townsend P D 2005 Structural and luminescence properties of Gd_2O_3:Eu^{3+} and $Y_3Al_5O_{12}$:Ce^{3+} phosphor particles synthesized via aerosol *J. Electrochem. Soc.* **152** 707–13

[5] Luff B J and Townsend P D 1993 High sensitivity thermoluminescence spectrometer *Meas. Sci. Technol.* **4** 65–71

[6] Morniroli J P and Steeds J W 1992 Microdiffraction as a tool for crystal structure identification and determination *Ultramicroscopy* **45** 219–39

[7] Tissue B M and Yuan H B 2003 Structure, particle size and annealing of gas-phase condensed Eu^{3+}:Y_2O_3 nanophosphors *J. Solid State Chem.* **171** 12–8

[8] Camenzind A, Strobel R and Pratsinis E 2005 Cubic or monoclinic Y_2O_3:Eu^{3+} nanoparticles by one step flame spray pyrolysis *Chem. Phys. Lett.* **415** 193–97

[9] Williams D K, Bihari B, Tissue B M and McHale J M 1998 Preparation and fluorescence spectroscopy of bulk monoclinic Eu^{3+}:Y_2O_3 and comparison to Eu^{3+}:Y_2O_3 nanocrystals *J. Phys. Chem.* B **102** 916–20

[10] Garcia-Murillo A, Le Luyer C, Grapon C, Dujardin C, Bernstein E, Pedrini C and Mugnier J 2002 Optical properties of europium-doped Gd_2O_3 waveguiding thin films prepared by the sol–gel method *Opt. Mater.* **19** 161–8

[11] Buijs M, Meyerink A and Blasse G 1987 Energy transfer between Eu^{3+} ions in a lattice with two different crystallographic sites: Y_2O_3:Eu^{3+}, Gd_2O_3:Eu^{3+} and Eu_2O_3 *J. Lumin.* **37** 9–20

[12] Pires A M, Davolos M R and Stucchi E B 2001 Eu^{3+} as a spectroscopic probe in phosphor based on spherical fine particle gadolinium compound *Int. J. Inorg. Mater.* **3** 785–90

[13] Rack P D and Holloway P H 1998 The structure, device physics and materials properties of thin film electroluminescent displays *Mater. Sci. Eng.* R **21** 171–219

[14] Townsend P D, Jazmati A K, Karali T, Maghrabi M, Raymond S G and Yang B 2001 Rare earth size effects on thermoluminescence and second harmonic generation *J. Phys.: Condens. Matter* **13** 2211–24

[15] Townsend P D 2001 How big is a point defect? *Radiat. Eff. Defects Solids* **155** 11–16

[16] Dujardin C, Ledoux G, Amans D and Mercier B 2006 Confinement effects in luminescent nano-insulators *Eurodim 2006: 10th Europhysical Conf. on Defects in Insulating Materials,*; *Phys. Status Solidi* c at press

[17] McKeever S W S, Moscovitch M and Townsend P D 1995 *Thermoluminescence Dosimetry Materials: Properties and Uses* (Ashford: Nuclear Technology Publishing)

[18] Calderon T, Townsend P D, Beneitez P, Garcia-Guinea J, Millan A, Rendell H M, Tookey A, Urbina M and Wood R A 1996 Crystal field effects on the thermoluminescence of manganese in carbonate lattices *Radiat. Meas.* **26** 719–31

[19] Yang B, Townsend P D and Rowlands A P 1998 Thermoluminescence of LaF_3 *Phys. Rev.* B **57** 178–88

[20] Yang B and Townsend P D 2000 Patterns of peak movement in rare earth doped lanthanum fluoride *J. Appl. Phys.* **88** 6395–402

[21] Raymond S G and Townsend P D 2000 The influence of rare earth ions on the low temperature thermoluminescence of $Bi_4Ge_3O_{12}$ *J. Phys.: Condens. Matter* **12** 2103–22